OXFORD

SOT | Society of Toxicology
academic.oup.com/toxsci

TOXICOLOGICAL SCIENCES, 177(1), 2020, 158–167

doi: 10.1093/toxsci/kfaa105
Advance Access Publication Date: 10 June 2020
Research Article

Drp-1-Dependent Mitochondrial Fragmentation Contributes to Cobalt Chloride-Induced Toxicity in *Caenorhabditis elegans*

Fuli Zheng ,*,†,1 Pan Chen,† Huangyuan Li ,*,1 and Michael Aschner†,1

*Department of Preventive Medicine, School of Public Health, Fujian Medical University, Fuzhou 350122, China and †Department of Molecular Pharmacology, Albert Einstein College of Medicine, Bronx, New York 10461

[1]To whom correspondence should be addressed at Department of Preventive Medicine, School of Public Health, Fujian Medical University, Fuzhou 350122, China. E-mails: f.zheng@fjmu.edu.cn and lhy@fjmu.edu.cn and Department of Molecular Pharmacology, Albert Einstein College of Medicine, Forchheimer 209, 1300 Morris Park Avenue, Bronx, NY 10461. E-mail: michael.aschner@einsteinmed.org.

ABSTRACT

Excess cobalt may lead to metallosis, characterized by sensorineural hearing loss, visual, and cognitive impairment, and peripheral neuropathy. In the present study, we sought to address the molecular mechanisms of cobalt-induced neurotoxicity, using *Caenorhabditis elegans* as an experimental model. Exposure to cobalt chloride for 2 h significantly decreased the survival rate and lifespan in nematodes. Cobalt chloride exposure led to increased oxidative stress and upregulation of glutathione S-transferase 4. Consistently, its upstream regulator *skn-1*, a mammalian homolog of the nuclear factor erythroid 2-related factor 2, was activated. Among the mRNAs examined by quantitative real-time polymerase chain reactions, apoptotic activator *egl-1*, proapoptotic gene *ced-9*, autophagic (*bec-1* and *lgg-1*), and mitochondrial fission regulator *drp-1* were significantly upregulated upon cobalt exposure, concomitant with mitochondrial fragmentation, as determined by confocal microscopy. Moreover, *drp-1* inhibition suppressed the cobalt chloride-induced reactive oxygen species generation, growth defects, and reduced mitochondrial fragmentation. Our novel findings suggest that the acute toxicity of cobalt is mediated by mitochondrial fragmentation and *drp-1* upregulation.

Key words: cobalt; toxicity; oxidative stress; mitochondria fragmentation; drp-1.

As a component of vitamin B12, cobalt is an essential metal for cellular growth, differentiation, and development (Bumoko *et al.*, 2015; Deshmukh *et al.*, 2013). However, excessive bodily cobalt can cause toxicity (Fowler, 2016; LiSon *et al.*, 2018). Excessive cobalt serum levels can arise from a variety of sources including natural erosion, diet, exposure during industrial fabrication, or from alloys used in tooth and hip joint replacements (Cheung *et al.*, 2016). High levels of cobalt may lead to metallosis, characterized by sensorineural hearing loss, visual, and cognitive impairment and peripheral neuropathy (Leyssens *et al.*, 2017). In Wistar rats, $CoCl_2$ overexposure results in several distinct defects, including hypoxia, lipid peroxidation, apoptosis, and the loss of learning, memory, and spatial-exploration (Akinrinde and Adebiyi, 2019; Zheng *et al.*, 2019). The transmission of $CoCl_2$ toxicity from parents to offspring in *Caenorhabditis elegans* has been reported by Wang *et al.*, affecting lifespan, development, chemotactic plasticity, and hsp16-associated stress response (Wang *et al.*, 2007).

$CoCl_2$ induces hypoxia and expression of hypoxia-inducible factor-1 in various cell types, accompanying toxicity (Karovic *et al.*, 2007). $CoCl_2$-induced hypoxia has been shown to alter the expression of angiogenesis and apoptotic genes, therefore contributing to tumorigenesis (Bahadori *et al.*, 2019; Rana *et al.*, 2019). A hypoxia-inducible factor-1-independent mediator BLMP-1 (named according to its mouse homolog B lymphocyte-induced maturation protein 1) has been identified and is necessary for

response to $CoCl_2$-induced hypoxia in *C. elegans* (Padmanabha *et al.*, 2015). In addition to hypoxia, we have previously shown that $CoCl_2$ induces oxidative stress (Zheng *et al.*, 2019).

Oxidative stress causes disturbance in mitochondrial homeostasis (Elfawy and Das, 2019). Mitochondria homeostasis, also known as dynamics, refers to the variations of shape of mitochondria. The tubular, elongated, interconnected mitochondrial networks are generated by fusion, whereas fission leads to the generation of discrete fragmented mitochondria (Diaz and Moraes, 2008). The balance between mitochondrial fission and fusion is of great importance for optimal energy generation and supply, and thus cell viability. In addition, mitochondrial fission and fusion have been proposed to play key roles in autophagy and mitophagy. Damaged mitochondria have been shown to be separated by fission, recognized by phagophore, and in turn forming autolysosome, which proceeds through mitophagy (Yoo and Jung, 2018). On the other hand, disruption of normal mitochondrial fission and fusion can also generate reactive oxygen species (ROS), thus leading to oxidative stress (Meyer *et al.*, 2017). The ROS-involving dysregulation of mitochondrial dynamics has been further suggested to contribute in metabolic regulation, type 2 diabetes, cardiovascular disease, cancer, and neurodegenerative diseases (Bhat *et al.*, 2015; Kim and Song, 2016; Rovira-Llopis *et al.*, 2017; Subramaniam and Chesselet, 2013; Vásquez-Trincado *et al.*, 2016). One of the main mediators of mitochondrial fission is Dynamin-Related Protein 1 (DRP-1) (Praefcke and McMahon, 2004). DRP-1 is also proapoptotic and mediates autophagy (Breckenridge *et al.*, 2008; Martinez *et al.*, 2018). *Caenorhabditis elegans* is a powerful *in vivo* model to study environmental pollutant-induced toxicity and mitochondrial gene-environment interactions, as mitochondrial functions along with many pathways are well conserved with those in humans (Byrne *et al.*, 2019; Maglioni and Ventura, 2016; Tsang and Lemire, 2003). Moreover, the *in vivo* study of mitochondrial structure and function is of considerable importance, as a large number of the regulating signals arise from diverse tissues and cell types, which are lost when studying in *in vitro* models (McBride *et al.*, 2006).

Therefore, in the present study, we sought to determine the molecular and mitochondrial mechanisms of $CoCl_2$-induced toxicity in *C. elegans*. We posited that in *C. elegans*, $CoCl_2$ induces toxicity through oxidative stress and mitochondrial fragmentation, secondary to the activation of DRP1. $CoCl_2$-induced toxicity in survival and lifespan was first established, followed by oxidative stress and mitochondrial morphology analyses. The role of *drp-1* in $CoCl_2$-induced toxicity was confirmed with *drp-1* mutant worms.

MATERIALS AND METHODS

Culture and maintenance of C. elegans *strains*. *Caenorhabditis elegans* strains, Bristol N2, CL2166 (*dvIs19 III*. [*Pgst-4p::GFP*]), VP596 (*dvIs19 III; vsIs33 V*. [[*Pgst-4p::GFP; Pdop-3::RFP*]), SD1347 (*ccIs4251 I*. [Pmyo-3p::GFP + Pmyo-3p::mitochondrial GFP]), CU6372 [*drp-1(tm1108)*], and *Escherichia coli* OP50, were procured from Caenorhabditis Genetics Centre (University of Minnesota, Minnesota), grown on nematode growth medium (NGM) and cultured at 20°C (Brenner, 1974). A synchronized population of nematodes was obtained by bleach treatment. Synchronized nematode cultures were initiated by bleaching gravid young adults and sucrose separation to obtain eggs (day 0). Sucrose flotation was included to remove potential contaminations such as residual dead debris and bacteria. Collected eggs were allowed to hatch overnight (approximately 18 h after plating) on unseeded NGM plates. The hatched larval stage 1 (L1) nematodes were used for experiments the next morning (day 1). For larval stage 4 (L4) experiments, L1-arrested larvae were transferred to 15-cm NGM plates seeded with OP50 *E. coli* on the late afternoon (day 1). On day 3 morning (40–44 h after plating), those nematodes will reach L4 (with the iconic half circle in the ventral side representing the developing vulva) and ready for experiments.

$CoCl_2$ exposure. $CoCl_2$ was used in this study to examine the toxicity of cobalt for its high bioavailability (defined as 100%) compared with other cobalt compounds, including Co_3O_4 and CoS (in the range of 0.06%–0.1%) (Danzeisen *et al.*, 2020). Moreover, $CoCl_2$ has been wildly used for cobalt toxicity determination in both *in vivo* and *in vitro* models (Bahadori *et al.*, 2019; Guan *et al.*, 2015; Rana *et al.*, 2019; Wang *et al.*, 2000, 2018). By choosing the same compound, our study afforded cross-species evaluation. Unless otherwise stated, all reagents were obtained from Sigma-Aldrich (St Louis, Missouri). A 2 M stock solution of $CoCl_2$ was prepared with ddH_2O. Because cobalt ion reacts with phosphate groups in M9 buffer and forms insoluble $Co_3(PO_4)_2$, 85 mM NaCl was used for $CoCl_2$ exposure. The 20× $CoCl_2$ exposure solutions of various doses were prepared using 85 mM NaCl. The exposure doses for nematodes were selected based on preliminary survival assays (0, 2.5, 5, 10, 25, and 50 mM). The doses are for acute liquid exposure (2 h), thus higher than the 0.1–4.76 mM in plates (solid exposure) for 12 h to 3 days previously reported in the literature (Chong *et al.*, 2009; Padmanabha *et al.*, 2015). After 2 washes with 85 mM NaCl, nematodes were exposed to $CoCl_2$ for 2 h. Due to the difference in sensitivity and size, 5000 L1 nematodes or 2500 L4 nematodes were exposed to $CoCl_2$ in 500 µl reaction system containing 25 µl of 20× $CoCl_2$ exposure solutions. This was followed by 2 washes with 85 mM NaCl to remove residual $CoCl_2$.

Survival assay. After $CoCl_2$ exposure from 0 to 100 mM and washed with 85 mM NaCl, approximately 30–40 nematodes were then transferred to 35 mm NGM plates freshly seeded with OP50 in triplicates. After incubation at 20°C for 24 h, nematodes were scored as alive or dead with a stereomicroscope (Stemi 2000, Zeiss, Germany). In some cases, dead nematodes were confirmed by touching the head region with the point of a platinum picker.

Measurement of ROS. After $CoCl_2$ exposure, 2′,7′-dichlorodihydrofluorescein diacetate/2′,7′-dichlorofluorescein (H_2DCFDA) was used to determine ROS in *C. elegans*. A previously published detailed method (Yoon *et al.*, 2018) was followed. Green fluorescence was measured by fluorescent plate reader (FluoStar OPTIMA, BMG LabTech) for up to 6 h.

Oxidative stress reporter assay. Activation of *skn-1*, the worm homolog of nuclear factor (erythroid-derived-2)-like 2 (*Nrf2*), was measured using CL2166 and VP596 strains, which expresses GFP under the control of the promoter for the *skn-1* target *GSH S-transferase 4* (*gst-4*). VP596 nematodes also express RFP under the *dop-3* promoter, serving as the loading control. After $CoCl_2$ exposure, GFP fluorescence of CL2166 nematodes was determined by a Leica SP8 Confocal Microscope and quantified by Fiji (Schindelin *et al.*, 2012). VP596 nematodes, on the other hand, were transferred to a 96-well black plate. Levels of RFP and GFP florescence were measured (RFP: excitation/emission 544/590 nm and GFP: 485/520 nm). GFP florescence was then divided by RFP florescence to normalize the data to worm number.

RNA isolation and quantitative real-time polymerase chain reactions. Ten thousand L1 nematodes or 2500 L4 nematodes per group were adequate for quantitative real-time polymerase chain reaction (qRT-PCR). mRNA was isolated with TRIzol following manufacture's protocol (Life Technologies, USA) with minor modifications. In brief, nematodes went through 3 freeze and thaw cycles with liquid nitrogen to breakdown cuticles and release RNA. The concentration and purity of the isolated RNA were determined by a NanoDrop 2000 spectrophotometer (Fisher, USA). cDNA was then reverse transcribed from RNA using High Capacity cDNA Reverse Transcription kit (Applied Biosystems, USA). Gene expression was detected by Taqman gene-expression assay probes (Thermo Fisher Scientific). Probes used in this study were Ce02412618_gH (*tba-1*); Ce02484980_g1 (*egl-1*); Ce02452076_g1 (*ced-9*); Ce02446175_g1 (*ced-4*); Ce02466776_m1 (*ced-3*); Ce02463990_m1 (*bec-1*); Ce02433594_g1 (*lgg-1*); Ce02407440_g1 (*drp-1*); Ce02433121_g1 (*fzo-1*); and Ce02463146_g1 (*miro-1*). The target gene expression was normalized to the relatively stable expression gene *tba-1* (Zhang *et al.*, 2012). The relative mRNA levels were determined with the $2^{-\triangle\triangle CT}$ method (Livak and Schmittgen 2001).

Mitochondrial imaging. Nematodes with mitochondria-tagged GFP proteins in body wall muscle (*ccIs4251 I*.) were used to assess alterations in mitochondrial morphology upon $CoCl_2$ exposure. Synchronized L4 larvae were treated with $CoCl_2$ for 2 h, followed by 1 h recovery. Worms were then anesthetized in 1 mM levamisole and then mounted onto a microscope slide containing a 4% agarose pad. Images were taken immediately after slide preparation to avoid artifact on a Leica SP8 Confocal Microscope with a 63× oil lens with excitation/emission wavelengths at 488/520 nm for GFP.

In additional experiments, nematodes were labeled with MitoTracker prior to imaging. Upon pilot experiments, we discovered that MitoTracker staining of the mitochondria and $CoCl_2$ exposure cannot be performed at the same time. When exposed to 10 mM of $CoCl_2$, only half of the nematodes had their mitochondria labeled. As the dose of $CoCl_2$ increased, the dye failed either to enter the worms or to target to the mitochondria (data not shown). Therefore, we stained the mitochondria prior to the $CoCl_2$ exposure. Nematode growth medium plates were freshly seeded with OP50 mixed with 5 μM MitoTracker red CMXRos (Invitrogen, Carlsbad, California). Synchronized L4 nematodes were grown on the plates overnight, followed by $CoCl_2$ exposure. Afterward, nematodes were recovered in clean seeded plates (without MitoTracker dye) for 1 h to remove all residue dyes in the gut. Fluorescence images were captured using a Nikon ECLIPSS 80i fluorescence microscope with a 60× oil lens.

Mitochondrial morphology was assessed in at least 30 animals analyzed for each condition and blindly scored. The morphological categories of mitochondria were defined according to Momma *et al.* (2017) with slight modification: (1) tubular: a majority of mitochondria were interconnected and elongated like tube shape, (2) intermediate: a combination of interconnected and fragmented mitochondria, and (3) fragmented: a majority of round or short mitochondria in the image taken.

Lifespan assay. L4 nematodes were exposed to 10 mM $CoCl_2$ for 2 h, then moved to fresh 3.5-cm NGM plates seeded with OP50 *E. coli* (lifespan experiment "day 0"). To prevent offspring from nematodes under study from reaching adulthood, fluorodeoxyuridine was added to OP50-spread NGM plates to a final concentration of 120 μM (Sutphin and Kaeberlein, 2009). A hundred and twenty nematodes were studied per strain, divided on two 35 mm NGM plates. Mortality was confirmed by poking nematodes lightly with a platinum wire (3 times) and monitoring them for at least 5 min; nematodes that did not move after stimulation were scored as dead and removed from the plate. Nematodes that died due to protruding/bursting vulva, bagging, or crawling off the agar were marked as "censored." In group WT-0, WT-10, *drp1 (tm1108)*-0, and *drp1 (tm1108)*-10, censored worms were 4, 5, 2, and 3, respectively. Therefore, the exact total *N* value for each group was > 114. Median, mean, and maximal lifespan were determined for each strain relative to concurrently studied wildtype nematodes.

Statistical analysis. Statistical analysis was performed using GraphPad PRISM, Version 8 (California, USA). Each experiment was repeated at least 3 times and normalized to unexposed groups. Analysis of variance followed by Tukey's or Dunnett's (where comparison was only to control) post hoc tests were utilized. For all experiments, $p < .05$ was deemed to be statistically significant. If not specifically stated, data are expressed as mean ± SD.

RESULTS

$CoCl_2$-Impaired Survival and -Induced Oxidative Stress in C. elegans

Upon $CoCl_2$ exposure, the survival of wildtype L1 *C. elegans* was reduced in a dose-dependent manner, with an LD_{50} (50% lethal dose) of 20.69 mM (Figure 1). A similar lethality pattern was also found in L4 nematodes (LD_{50}: 29.98 mM) (Figure 5A). At higher doses where survival was significantly reduced compared with controls, a portion of worms displayed health defects, their bodies straightened and/or failing to move (extreme sluggishness) (Supplementary Figure S2).

$CoCl_2$-induced oxidative stress in *C. elegans* was detected with the H_2DCFDA assay. H_2DCFDA, the cell permeant fluorescent probe, is rapidly oxidized in the presence of ROS to highly fluorescent DCF. Therefore, an increase in the fluorescence signal is deemed to positively correlate with increased intracellular ROS generation (Labuschagne and Brenkman, 2013). Although 5 and 10 mM $CoCl_2$ failed to alter survival (Figure 1A), both doses significantly induced ROS generation (Figure 1B). These results establish that $CoCl_2$ induced both lethality and oxidative stress in *C. elegans*.

Skn-1-Involved Oxidative Stress Defense System Is Activated by $CoCl_2$

Skn-1, the mammalian homolog of nuclear factor E2-related factor 2 (*Nrf2*), is a master regulators of oxidative stress defense systems. Because *gst-4* is a main downstream target of *skn-1*, we used a *gst-4::GFP* strain (CL2166) to evaluate *skn-1* activation (using GFP readout). Upon $CoCl_2$ exposure, fluorescence was significantly upregulated (Figure 2A). Fluorescent intensities were significantly increased in worms treated with 5 and 10 mM $CoCl_2$ (Figure 2B). Corroborative evidence of *gst-4*-induced GFP expression upon $CoCl_2$ exposure can be found in Supplementary Figure S2, using the VP596 strain. qRT-PCR (Figure 2C) of *skn-1* confirmed that oxidative stress defense in the nematode is activated upon $CoCl_2$ exposure.

Apoptotic, Autophagic, and Mitochondrial Structure Regulators Are Activated Upon $CoCl_2$ Exposure

Next, we addressed additional physiological changes at the gene-expression level of $CoCl_2$ exposure in *C. elegans*. As shown

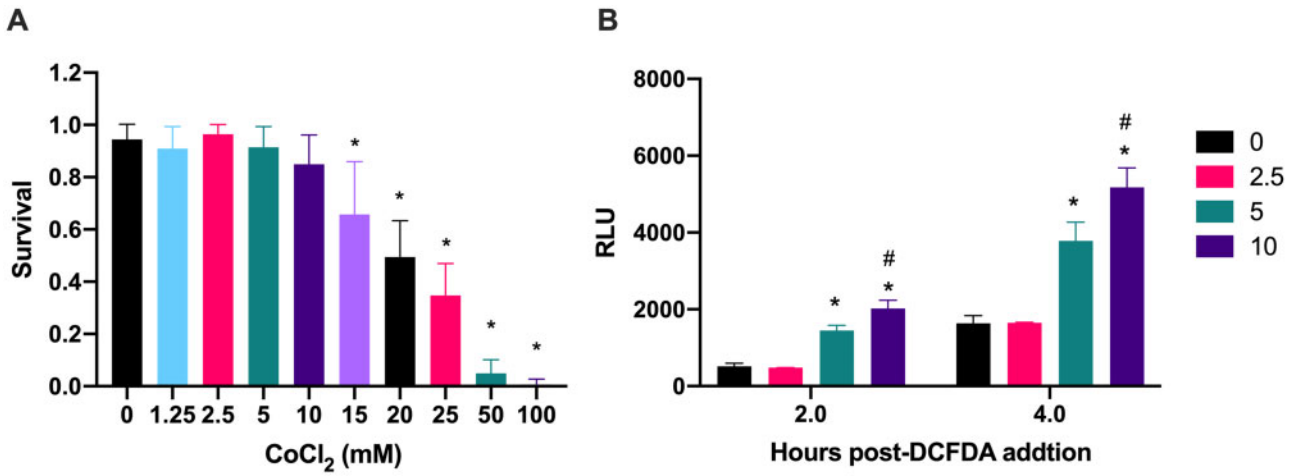

Figure 1. $CoCl_2$ exposure induces lethality and oxidative stress in *Caenorhabditis elegans*. A, L1 nematodes were exposed to $CoCl_2$ at various doses for 2 h. $N = 3$ with more than 30 animals per plate. Individual experiment was repeated for 5 times. B, L1 animals exposed to $CoCl_2$ (0, 2.5, 5, and 10 mM), were detected by 2′,7′-dichlorodihydrofluorescein diacetate/2′,7′-dichlorofluorescein assay. Fluorescence was followed every 0.5 h for 6 h, with representative 2 and 4 h shown here ($N = 3$). Individual experiments were independently repeated for 3 times. $^{*}p < .05$ compared with 0 mM $CoCl_2$. $^{\#}p < .05$ compared with 5 mM Co group.

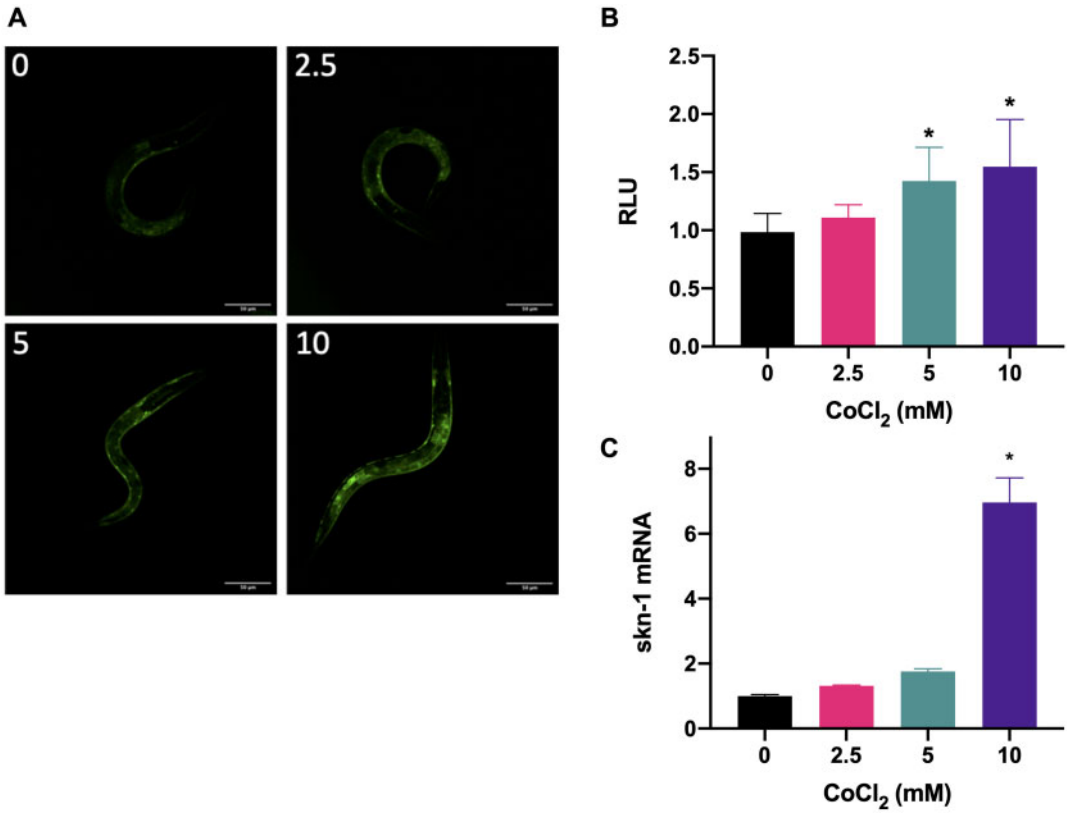

Figure 2. Oxidative stress defense system is turned on by $CoCl_2$. A, Worms with oxidative stress inducible *gst-4p::GFP* were exposed to $CoCl_2$ for 2 h and detected by confocal microscopy. Bar indicates 50 μm. B, Fluorescent intensities of at least 30 animals were quantified by Fiji. C, *Skn-1* mRNA, the activator of *gst-4*, is increased ($N = 3$ with 10 000 animals per sample). Individual experiments were independently repeated for 4 times. $^{*}p < .05$ compared with 0 mM $CoCl_2$.

in Figure 3, $CoCl_2$ significantly increased the expression of apoptosis-associated genes, namely *egl-1*, *ced-9*, and *ced-3* (homologous of mammalian *Bh3*, *Bcl-2*, and *Caspase-9*, respectively). Moreover, autophagic hallmarks such as the *ATG6* ortholog *bec-1*, as well as the *LC3* homolog, *lgg-1*, were significantly induced by $CoCl_2$.

Mitochondrion is not only a critical compartment where ROS are generated but also a key organelle in mediating apoptosis and autophagy (Bloemberg and Quadrilatero, 2019; Kwon *et al.*, 2018). Increased mitochondrial fission by elevated ROS production could facilitate autophagy (Huang *et al.*, 2016). Thus, we determined whether mitochondrial fission and fusion were in responsible for the augmented autophagy. In response to $CoCl_2$ exposure, the mitochondrial fission regulator, *drp-1*, was upregulated, but mRNA levels of mitochondrial fusion, such as *fzo-1* and *miro-1*, were indistinguishable from control (Figure 3).

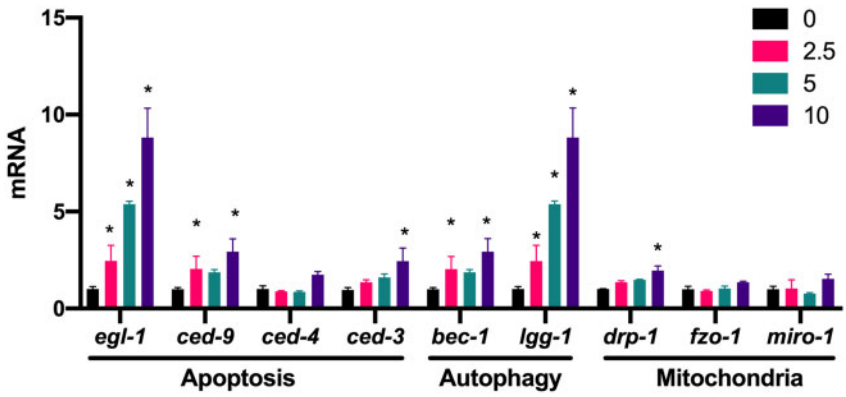

Figure 3. Apoptotic, autophagic, and mitochondrial morphologic regulators are activated upon $CoCl_2$ exposure. mRNAs were isolated from L1 animals exposed to $CoCl_2$ (0, 2.5, 5, and 10 mM) for 2 h. Apoptosis, autophagy, and mitochondrial morphology-associated genes were examined by quantitative real-time polymerase chain reaction. mRNA levels were normalized to *tba-1* ($N = 3$, 10 000 animals per sample). Individual experiments were independently repeated for 4 times. $^*p < .05$ compared with 0 mM $CoCl_2$. Experiments were performed in L4 animals with analogous results.

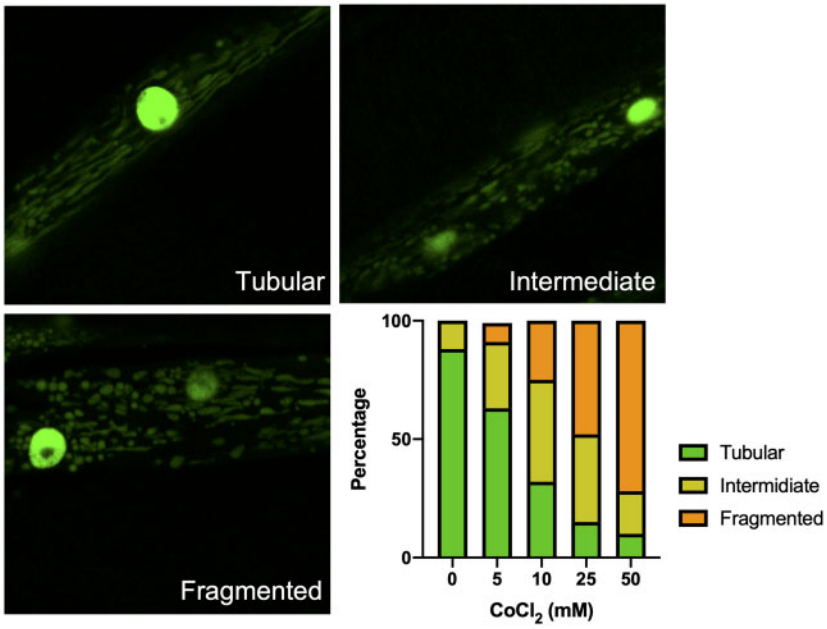

Figure 4. $CoCl_2$ induces mitochondrial fission. L4 nematodes were exposed to $CoCl_2$ at various doses for 2 h, then examined by fluorescent microscopy ($N > 30$). Mitochondrial morphology was classified into 3 categories: tubular, intermediate, and fragmented. All exposure groups are significantly different to control group ($p < .01$), examined by Chi-square test. Individual experiments were independently repeated for 3 times.

Mitochondrial Fragmentation Upon $CoCl_2$ Exposure

Based on the expression changes of mitochondrial dynamic regulators, next, we examined whether the mitochondrial morphology was altered upon $CoCl_2$ exposure using a fluorescent-labeled mitochondria strain, SD1347. In order to better identify the mitochondrial morphology changes, L4 and young adult nematodes were used. In controls, the majority of the mitochondria assumed a tubular shape. $CoCl_2$ induced alterations in mitochondrial morphology at doses as low as 5 mM. Corroborating the upregulated *drp-1* data, a greater number of fragmented mitochondria were observed as the dose of $CoCl_2$ increased (Figure 4).

Drp-1 Suppression Alleviated $CoCl_2$-Induced Growth Defects

To address the causal relationship between *drp-1*-induced mitochondrial fragmentation and $CoCl_2$-induced damage, we utilized a *drp-1* mutant strain. Upon 50 mM $CoCl_2$ exposure, a greater percentage of *drp-1* mutants (43.13%) survived compared with WT nematodes (26.98%) (Figure 5A). For lifespan studies, a lower dose of $CoCl_2$ was selected to eliminate the acute effects and prolong survival. As shown in Figure 5B, lifespan in WT worms was shortened upon $CoCl_2$ exposure at the L4 stage. Median survival of WT control and WT-$CoCl_2$ was 12 and 10 days, respectively. In the absence of $CoCl_2$, the lifespan of *drp-1* mutants was statistically indistinguishable from WT nematodes. However, upon $CoCl_2$ exposure, *drp-1* mutants had significantly longer lifespan compared with WT nematodes (Figure 5B). This was supported by the median survival for *drp1*-$CoCl_2$: 11 days. Thus, *drp-1* mutation reduces the $CoCl_2$-induced decrease in survival and lifespan.

Drp-1 Is Essential for $CoCl_2$-Induced Mitochondrial Fission and ROS Generation

Finally, we determined whether *drp-1* has a role in mitochondrial fission, given that *drp-1* mutants were less vulnerable to $CoCl_2$-induced toxicity. Studies on lifespan and behavior of the

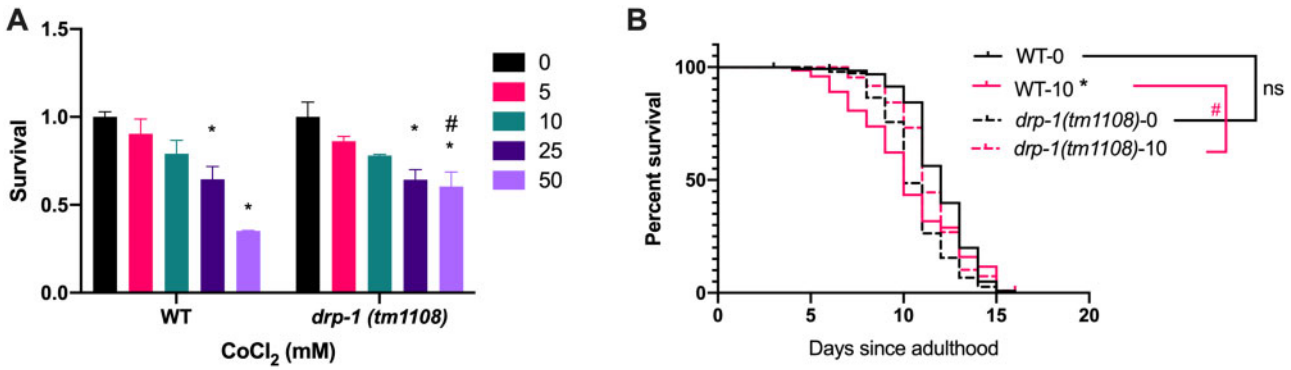

Figure 5. Inhibition of mitochondrial fission regulator DRP1 rescues cell growth and extends life span in nematodes upon $CoCl_2$ exposure. L4 *drp-1 (tm1108)* null mutant strain was exposed to $CoCl_2$ of various doses for 2 h, in line with WT strain. A, *Drp-1* inhibition rescued lethality in 50 mM $CoCl_2$ exposure group ($N = 3$, at least 30 animals per replicate). $^{*}p < .05$ compared with unexposed nematodes. $^{\#}p < .05$ compared WT-$CoCl_2$ with *drp-1*-$CoCl_2$. B, *Drp-1* suppression extended lifespan in response to 10 mM $CoCl_2$ exposure ($N = 106$, 105, 108, and 107 for WT-0, WT-10, *drp-1*-0, and *drp-1*-10, respectively). $^{*}p < .0001$ compared with unexposed nematodes. $^{\#}p = .0042$ compared WT-$CoCl_2$ with *drp-1*-$CoCl_2$, examined by log-rank method (Mantel-Cox method). Individual experiments were independently repeated for 3 times for survival and 4 times for lifespan.

drp-1 mutant strain have shown unchanged or extended lifespan (Byrne *et al.*, 2019), but none has addressed lifespan in this mutant strain upon $CoCl_2$ exposure. We examined mitochondrial morphology in both WT and *drp-1* mutants upon $CoCl_2$ exposure (Figure 6A). At the tested doses, *drp-1* mutants displayed higher percentage of tubular to intermediate mitochondria in response to $CoCl_2$ exposure, whereas WT nematodes displayed more fragmented mitochondria (Figure 6B). Thus, *drp-1* mutation negatively correlates with $CoCl_2$-induced mitochondrial fission.

Mitochondrial fission and fusion dysregulation has been suggested to result in ROS and thus mitochondrial toxicity (Meyer *et al.*, 2017). To further determine the potential mechanism of *drp-1* in $CoCl_2$-induced toxicity, we measured the ROS level in both WT and *drp-1* mutants. Corroborating L1 result (Figure 1B), $CoCl_2$ induced ROS in L4 animals. However, the induction of ROS was not evident in *drp-1* mutants (Figure 6C). Thus, our results suggest that *drp-1* mutation suppresses ROS generation upon $CoCl_2$ exposure.

DISCUSSION

Here, we demonstrate for the first time, that in the nematode, acute $CoCl_2$ exposure induces toxicity (growth defects, oxidative stress, apoptosis, and autophagy) by mitochondrial fragmentation. The activation of *drp-1*, the inducer of outer mitochondrial membrane fission, leads to ROS production and mitochondrial toxicity.

Cobalt induces toxicity in various organisms and tissues. In patients with hip replacement, cobalt levels have been shown to be 1.8-fold higher than in controls, concomitant with neurodegenerative changes (Catalani *et al.*, 2012; Leyssens *et al.*, 2017; Wu *et al.*, 2018). We have previously demonstrated that oxidative stress is a key mediator of the toxicity of cobalt and its nanoparticles, both in rats and PC12 cells (Zheng *et al.*, 2019). Moreover, the activation of *Nrf2*, the mammalian homolog of *skn-1*, and its protective role in $CoCl_2$-induced toxicity, has been established. In rat liver, microarray and mass spectrometry analysis studies have shown that exposure to $CoCl_2$ causes transcriptomic and proteomic changes, including Nrf2-mediated response and glutathione (GSH) generation, consistent with an oxidative stress response (Permenter *et al.*, 2013). Overexpression of *Nrf2* in mesenchymal stem cells has been shown to prevent $CoCl_2$-induced apoptosis, maintaining stemness (Yuan *et al.*, 2017). In human keratinocytes, *Nrf2* has been shown in the antioxidant response upon $CoCl_2$ treatment (Yang *et al.*, 2018). Downstream targets of the Nrf2/ARE pathway, such as *mfat-1*, have been shown to protect cultured adult neural stem cell against $CoCl_2$-mediated hypoxia injury (Yu *et al.*, 2018a). Here, we found activation of *skn-1* and its downstream target *gst-4* upon $CoCl_2$ exposure in *C. elegans*, consistent with the involvement of oxidative stress and *Nrf2* defense systems in the acute response to this metal. Our results provide *in vivo* evidence in support of the involvement of ROS and the activation of *skn-1* in $CoCl_2$-induced toxicity.

Moreover, we have observed the upregulation of apoptotic activator *egl-1* and proapoptotic *ced-4* upon $CoCl_2$ exposure. In agreement, apoptosis induced by $CoCl_2$ has been noted in *C. elegans* germline cells and rats, concomitant with increased *Bax/Bcl-2* ratio and activation of *Caspase 9* (Chong *et al.*, 2009; Wang *et al.*, 2018; Zheng *et al.*, 2019). In addition to apoptosis, our study has shown the induction of autophagy upon $CoCl_2$ exposure. A close link exists between apoptosis and autophagy upon cellular stress. For example, inhibition of autophagy enhances apoptosis in response to $CoCl_2$ in rats lung cells (Yu *et al.*, 2018b). Our *in vivo* results further corroborate this link because both apoptosis and autophagy were affected by $CoCl_2$. Autophagy, especially mitophagy, a type of macroautophagy that selectively degrades damaged mitochondria, might be an outcome of mitochondrial fission (Yoo and Jung, 2018).

Here, we have observed mitochondrial fragmentation in response to $CoCl_2$ exposure, consistent with the upregulation of *drp-1* mRNA. Mitochondrial homeostasis is regulated by 2 sets of genes, the fission inducer (*drp-1*) and the fusion mediator (*mfn-1/2* and *miro-1*), the latter homologous to *fzo-1* and *miro-1* in *C. elegans*. Mitochondrial fragmentation is a signal for mitochondrial dysfunction, which is prone to apoptosis and cell death (Byrne *et al.*, 2019; Momma *et al.*, 2017; Sebastian *et al.*, 2017). Fusion-deficient nematodes were more sensitive to toxicants, including aflatoxin B1, arsenite, cisplatin, paraquat, and rotenone, suggesting that mitochondrial fusion is essential for cellular responses to toxic effects (Hartman *et al.*, 2019; Luz *et al.*, 2017). Moreover, *drp-1*-induced mitochondrial fragmentation in response to ethanol exposure has been demonstrated to contribute to the activation of the mitochondrial unfolded protein response (Oh *et al.*, 2020). Here, we found that when *drp-1* was

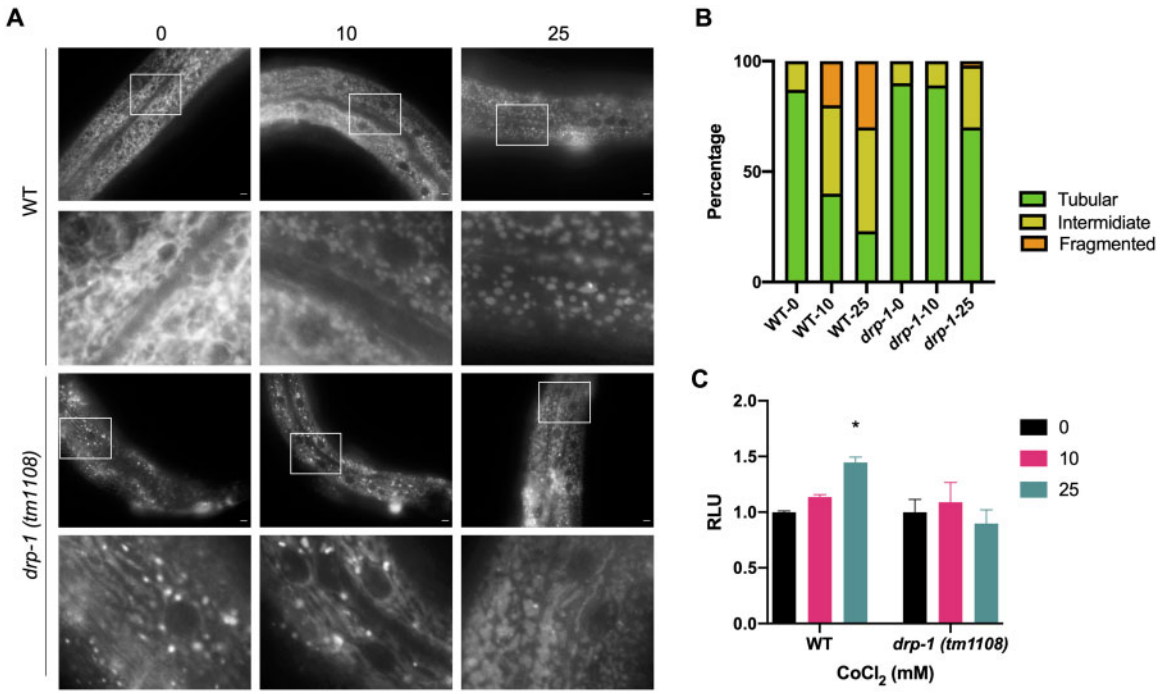

Figure 6. Reduced mitochondrial fission and elevated reactive oxygen species production in *drp-1 (tm1108)* mutant upon $CoCl_2$ exposure. A, WT and *drp-1* mutant strains were stained with MitoTracker red CMXRos overnight, followed by $CoCl_2$ exposure of 0, 10, and 25 mM. Mitochondrial morphology was examined using fluorescent microscopy. Bar indicates 5 μm. The lower panel shows the enlarged areas as boxed in the upper panel within each strain ($N > 30$). B, Quantification of mitochondrial morphology to tubular, intermediate, and fragmented. WT-10 and WT-25 are significantly different to WT-0, whereas *drp-1*-25 is significantly different to WT-0 and *drp-1*-0 ($p < .01$), examined by Chi-square test. Individual experiments were independently repeated for 3 times. C, L4 animals exposed to $CoCl_2$ (0, 10, and 25 mM), were detected by 2′,7′-dichlorodihydrofluorescein diacetate/2′,7′-dichlorofluorescein assay. Fluorescence was followed with 2 h RLU data shown here (cobalt-untreated group was set to 1) ($N = 3$). Individual experiments were independently repeated in triplicates. $^*p < .05$ compared with 0 mM $CoCl_2$.

mutated, the $CoCl_2$-induced defects including lethality, reduced lifespan, and increased ROS generation were no longer observed, concomitant with reduced mitochondrial fragmentation in nematodes. Similarly, in rat astrocytoma C6 cells, inhibition of *drp-1* reduced the number of apoptotic nuclei and preserved the integrity of the mitochondrial network, thus prevented Mn-induced cell death (Alaimo *et al.*, 2014). In rhabdomyolysis-induced acute kidney injury, reduced *drp-1* protein accumulation in mitochondria ameliorated mitochondrial injury and apoptosis (Tang *et al.*, 2013). An opposite effect was noted in the rat hippocampus upon *drp-1* inhibition by synthetic xenoestrogen bisphenol A (Agarwal *et al.*, 2016). Moreover, overexpressing Opa-1, the fusion protein, prevented drp-1-dependent mitochondrial fragmentation in SH-SY5Y cells overexpressing α-synuclein, an *in vitro* model of Parkinson's disease (Martinez *et al.*, 2018). In human lung bronchial epithelial cells, the antioxidant quercetogetin inhibited cigarette smoke extract-induced mitochondrial dysfunction and mitophagy secondary to the inhibition of phospho-DRP-1 and PINK1 (Son *et al.*, 2018), corroborating our findings that *drp-1* mutants fail to show changes in ROS production upon $CoCl_2$ exposure.

Taken together, these results suggest that $CoCl_2$ induces *drp-1*-associated mitochondrial fragmentation, in turn, causing ROS production and detrimental defects (Figure 7). Mitochondrial dysfunction is correlated with neurodegenerative processes (Itoh *et al.*, 2013), suggesting that $CoCl_2$-induced mitochondrial dysfunction may trigger neurodegenerative changes associated with joint replacements in patients.

Other possible mechanisms associated with *drp-1* inactivation that extend lifespan should be considered; they include (1) the reduction of insulin signaling by *drp-1* suppression (Yang *et al.*, 2011) and (2) the proapoptotic function of *drp-1* downstream of *ced-3* (Breckenridge *et al.*, 2008). Accordingly, future studies should address the role of *drp-1* in regulating the link between apoptosis and autophagy. A reverse mutation assay by introducing *drp-1* back to the *drp-1* mutants would be profitable in addressing this issue. Moreover, additional studies are required to determine the role of altered mitochondrial function in mediating $CoCl_2$-induced neurodegenerative changes. Moreover, we would like to point out that the mild effects of *drp-1* inactivation seen herein could be explained by the involvement of other mitochondrial dynamic regulators such as *fzo-1 and eat-3 (fusion)* or *miro-1* (mitochondrial transport and localization). Mutations in *fzo-1* or *eat-3* have been previously shown to significantly reduce the median lifespan of worms (Byrne *et al.*, 2019; Luz *et al.*, 2017). The disruption of *miro-1* reduces the number of mitochondria by half and extends life span (Shen *et al.*, 2016). These studies indicate potential roles for *fzo-1*, *eat-3*, *and miro-1* in $CoCl_2$-induced lifespan alterations. Combined with our mRNA results showing that *fzo-1* and *miro-1* remains unchanged, the proposed regulation of *drp-1* is most likely at translational or posttranslational level. Further explorations of these genes upon $CoCl_2$ exposure are clearly warranted.

In summary, our novel findings show that in nematodes, $CoCl_2$ exposure is associated with increased lethality and oxidative stress, as well as activation of autophagy and induction of apoptosis. Furthermore, $CoCl_2$ exposure causes mitochondrial fragmentation in *C. elegans* via the activation of *drp-1*, the inducer of mitochondrial fission. Inhibition of mitochondrial fission by *drp-1* mutation rescues the $CoCl_2$-induced growth defects and mitochondrial fission. Our work establishes the

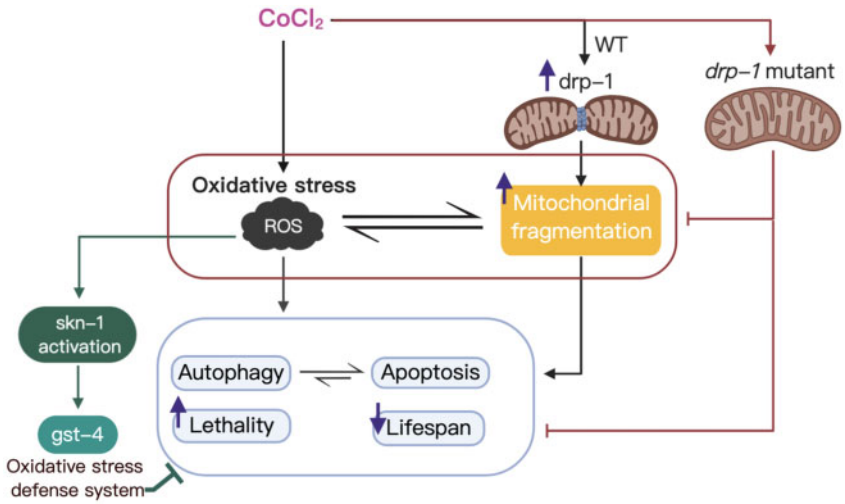

Figure 7. A model for $CoCl_2$-induced toxicity in *C. elegans*. $CoCl_2$ induces oxidative stress, followed by altered apoptosis, increased lethality, and reduced lifespan. Increased reactive oxygen species (ROS) generation leads to *skn-1* (Nrf2 homolog) activation and its downstream target *gst-4*, corroborating the involvement of oxidative stress defense systems (in green). $CoCl_2$ upregulates *drp-1* and induces mitochondrial fragmentation. Mitochondrial impairment is likely caused by oxidative stress from ROS generation. When *drp-1* is inhibited, mitochondrial fragmentation and ROS generation are suppressed, rescuing the $CoCl_2$-induced growth defects.

relevance of oxidative stress and mitochondrial homeostasis to the pathogenesis of cobalt-induced toxicity.

SUPPLEMENTARY DATA

Supplementary data are available at *Toxicological Sciences* online.

DECLARATION OF CONFLICTING INTERESTS

The authors declared no potential conflicts of interest with respect to the research, authorship, and/or publication of this article.

FUNDING

NCI Cancer Center support grant (P30CA013330) and a shared instrumentation grant (1S10OD023591-01) for the use of Leica SP8 Confocal Microscope; National Institutes of Health (Grant Nos. R01ES07331 and R01ES10563); the National Natural Science Foundation of China (Grant Nos. 81903352 and 81973083); the Provincial Natural Science Foundation of Fujian Province (Grant No. 2019J05081); the high-level personnel research startup funding of Fujian Medical University (Grant No. XRCZX2018002); Sailing Funding of Fujian Medical University (Grant No. 2017XQ1010); and the Joint Funds for the Innovation of Science and Technology, Fujian province (Grant No. 2017Y9105).

ACKNOWLEDGMENT

We like to thank Andrea Briceno (Analytical Imaging Facility, Albert Einstein College of Medicine) for her training of the microscope.

REFERENCES

Agarwal, S., Yadav, A., Tiwari, S. K., Seth, B., Chauhan, L. K., Khare, P., Ray, R. S., and Chaturvedi, R. K. (2016). Dynamin-related protein 1 inhibition mitigates bisphenol A-mediated alterations in mitochondrial dynamics and neural stem cell proliferation and differentiation. *J. Biol. Chem.* **291**, 15923–15939.

Akinrinde, A. S., and Adebiyi, O. E. (2019). Neuroprotection by luteolin and gallic acid against cobalt chloride-induced behavioural, morphological and neurochemical alterations in Wistar rats. *Neurotoxicology* **74**, 252–263.

Alaimo, A., Gorojod, R. M., Beauquis, J., Muñoz, M. J., Saravia, F., and Kotler, M. L. (2014). Deregulation of mitochondria-shaping proteins Opa-1 and Drp-1 in manganese-induced apoptosis. *PLoS One* **9**, e91848.

Bahadori, M. B., Vandghanooni, S., Dinparast, L., Eskandani, M., Ayatollahi, S. A., Ata, A., and Nazemiyeh, H. (2019). Triterpenoid corosolic acid attenuates HIF-1 stabilization upon cobalt (II) chloride-induced hypoxia in A549 human lung epithelial cancer cells. *Fitoterapia* **134**, 493–500.

Bhat, A. H., Dar, K. B., Anees, S., Zargar, M. A., Masood, A., Sofi, M. A., and Ganie, S. A. (2015). Oxidative stress, mitochondrial dysfunction and neurodegenerative diseases; a mechanistic insight. *Biomed. Pharmacother.* **74**, 101–110.

Bloemberg, D., and Quadrilatero, J. (2019). Autophagy, apoptosis, and mitochondria: Molecular integration and physiological relevance in skeletal muscle. *Am. J. Physiol. Cell Physiol.* **317**, C111–C130.

Breckenridge, D. G., Kang, B. H., Kokel, D., Mitani, S., Staehelin, L. A., and Xue, D. (2008). *Caenorhabditis elegans* drp-1 and fis-2 regulate distinct cell-death execution pathways downstream of ced-3 and independent of ced-9. *Mol. Cell* **31**, 586–597.

Brenner, S. (1974). The genetics of *Caenorhabditis elegans*. *Genetics* **77**, 71–94.

Bumoko, G. M., Sadiki, N. H., Rwatambuga, A., Kayembe, K. P., Okitundu, D. L., Mumba Ngoyi, D., Muyembe, J. J., Banea, J. P., Boivin, M. J., and Tshala-Katumbay, D. (2015). Lower serum levels of selenium, copper, and zinc are related to neuromotor impairments in children with konzo. *J. Neurol. Sci.* **349**, 149–153.

Byrne, J. J., Soh, M. S., Chandhok, G., Vijayaraghavan, T., Teoh, J. S., Crawford, S., Cobham, A. E., Yapa, N. M. B., Mirth, C. K., and Neumann, B. (2019). Disruption of mitochondrial

dynamics affects behaviour and lifespan in *Caenorhabditis elegans*. *Cell. Mol. Life Sci.* **76**, 1967–1985.

Catalani, S., Rizzetti, M., Padovani, A., and Apostoli, P. (2012). Neurotoxicity of cobalt. *Hum. Exp. Toxicol.* **31**, 421–437.

Cheung, A. C., Banerjee, S., Cherian, J. J., Wong, F., Butany, J., Gilbert, C., Overgaard, C., Syed, K., Zywiel, M. G., Jacobs, J. J., *et al.* (2016). Systemic cobalt toxicity from total hip arthroplasties: Review of a rare condition part 1—History, mechanism, measurements, and pathophysiology. *Bone Joint J.* **98-B**, 6–13.

Chong, R., Ke-zhou, C., and Zeng-liang, Y. (2009). Induction of germline apoptosis by cobalt and relevant signal transduction pathways in *Caenorhabditis elegans*. *Toxicol. Mech. Methods* **19**, 541–546.

Danzeisen, R., Williams, D. L., Viegas, V., Dourson, M., Verberckmoes, S., and Burzlaff, A. (2020). Bioelution, bioavailability, and toxicity of cobalt compounds correlate. *Toxicol. Sci.* **174**, 311–325.

Deshmukh, U., Katre, P., and Yajnik, C. S. (2013). Influence of maternal vitamin B12 and folate on growth and insulin resistance in the offspring. *Nestle Nutr. Inst. Workshop Ser.* **74**, 145154; discussion 154–146.

Diaz, F., and Moraes, C. T. (2008). Mitochondrial biogenesis and turnover. *Cell Calcium* **44**, 24–35.

Elfawy, H. A., and Das, B. (2019). Crosstalk between mitochondrial dysfunction, oxidative stress, and age related neurodegenerative disease: etiologies and therapeutic strategies. *Life Sci.* **218**, 165–184.

Fowler, J. F. Jr. (2016). Cobalt. *Dermatitis* **27**, 3–8.

Guan, D., Su, Y., Li, Y., Wu, C., Meng, Y., Peng, X., and Cui, Y. (2015). Tetramethylpyrazine inhibits $CoCl_2$-induced neurotoxicity through enhancement of Nrf2/GCLc/GSH and suppression of HIF1α/NOX2/ROS pathways. *J. Neurochem.* **134**, 551–565.

Hartman, J. H., Gonzalez-Hunt, C., Hall, S. M., Ryde, I. T., Caldwell, K. A., Caldwell, G. A., and Meyer, J. N. (2019). Genetic defects in mitochondrial dynamics in *Caenorhabditis elegans* impact ultraviolet c radiation- and 6-hydroxydopamine-induced neurodegeneration. *Int. J. Mol. Sci.* **20**, 3202.

Huang, Q., Zhan, L., Cao, H., Li, J., Lyu, Y., Guo, X., Zhang, J., Ji, L., Ren, T., An, J., *et al.* (2016). Increased mitochondrial fission promotes autophagy and hepatocellular carcinoma cell survival through the ROS-modulated coordinated regulation of the NFKB and TP53 pathways. *Autophagy* **12**, 999–1014.

Itoh, K., Nakamura, K., Iijima, M., and Sesaki, H. (2013). Mitochondrial dynamics in neurodegeneration. *Trends Cell Biol.* **23**, 64–71.

Karovic, O., Tonazzini, I., Rebola, N., Edström, E., Lövdahl, C., Fredholm, B. B., and Daré, E. (2007). Toxic effects of cobalt in primary cultures of mouse astrocytes: Similarities with hypoxia and role of HIF-1α. *Biochem. Pharmacol.* **73**, 694–708.

Kim, B., and Song, Y. S. (2016). Mitochondrial dynamics altered by oxidative stress in cancer. *Free Radic. Res.* **50**, 1065–1070.

Kwon, S., Kim, E. J. E., and Lee, S. V. (2018). Mitochondria-mediated defense mechanisms against pathogens in *Caenorhabditis elegans*. *BMB Rep.* **51**, 274–279.

Labuschagne, C. F., and Brenkman, A. B. (2013). Current methods in quantifying ROS and oxidative damage in *Caenorhabditis elegans* and other model organism of aging. *Ageing Res. Rev.* **12**, 918–930.

Leyssens, L., Vinck, B., Van Der Straeten, C., Wuyts, F., and Maes, L. (2017). Cobalt toxicity in humans—A review of the potential sources and systemic health effects. *Toxicology* **387**, 43–56.

Lison, D., van den Brule, S., and Van Maele-Fabry, G. (2018). Cobalt and its compounds: Update on genotoxic and carcinogenic activities. *Crit. Rev. Toxicol.* **48**, 522–539.

Livak, K. J., and Schmittgen, T. D. (2001). Analysis of relative gene expression data using real-time quantitative PCR and the 2(−delta C(t)) method. *Methods* **25**, 402–408.

Luz, A. L., Godebo, T. R., Smith, L. L., Leuthner, T. C., Maurer, L. L., and Meyer, J. N. (2017). Deficiencies in mitochondrial dynamics sensitize *Caenorhabditis elegans* to arsenite and other mitochondrial toxicants by reducing mitochondrial adaptability. *Toxicology* **387**, 81–94.

Maglioni, S., and Ventura, N. (2016). *C. elegans* as a model organism for human mitochondrial associated disorders. *Mitochondrion* **30**, 117–125.

Martinez, J. H., Alaimo, A., Gorojod, R. M., Porte Alcon, S., Fuentes, F., Coluccio Leskow, F., and Kotler, M. L. (2018). Drp-1 dependent mitochondrial fragmentation and protective autophagy in dopaminergic SH-SY5Y cells overexpressing alpha-synuclein. *Mol. Cell. Neurosci.* **88**, 107–117.

McBride, H. M., Neuspiel, M., and Wasiak, S. (2006). Mitochondria: More than just a powerhouse. *Curr. Biol.* **16**, R551–R560.

Meyer, J. N., Leuthner, T. C., and Luz, A. L. (2017). Mitochondrial fusion, fission, and mitochondrial toxicity. *Toxicology* **391**, 42–53.

Momma, K., Homma, T., Isaka, R., Sudevan, S., and Higashitani, A. (2017). Heat-induced calcium leakage causes mitochondrial damage in *Caenorhabditis elegans* body-wall muscles. *Genetics* **206**, 1985–1994.

Oh, K. H., Sheoran, S., Richmond, J. E., and Kim, H. (2020). Alcohol induces mitochondrial fragmentation and stress responses to maintain normal muscle function in *Caenorhabditis elegans*. *FASEB J.* **34**, 8204–8216.

Padmanabha, D., Padilla, P. A., You, Y.-J., and Baker, K. D. (2015). A HIF-independent mediator of transcriptional responses to oxygen deprivation in *Caenorhabditis elegans*. *Genetics* **199**, 739–748.

Permenter, M. G., Dennis, W. E., Sutto, T. E., Jackson, D. A., Lewis, J. A., and Stallings, J. D. (2013). Exposure to cobalt causes transcriptomic and proteomic changes in two rat liver derived cell lines. *PLoS One* **8**, e83751.

Praefcke, G. J., and McMahon, H. T. (2004). The dynamin superfamily: Universal membrane tubulation and fission molecules? *Nat. Rev. Mol. Cell Biol.* **5**, 133–147.

Rana, N. K., Singh, P., and Koch, B. (2019). $CoCl_2$ simulated hypoxia induce cell proliferation and alter the expression pattern of hypoxia associated genes involved in angiogenesis and apoptosis. *Biol. Res.* **52**, 12.

Rovira-Llopis, S., Bañuls, C., Diaz-Morales, N., Hernandez-Mijares, A., Rocha, M., and Victor, V. M. (2017). Mitochondrial dynamics in type 2 diabetes: Pathophysiological implications. *Redox Biol.* **11**, 637–645.

Schindelin, J., Arganda-Carreras, I., Frise, E., Kaynig, V., Longair, M., Pietzsch, T., Preibisch, S., Rueden, C., Saalfeld, S., Schmid, B., *et al.* (2012). Fiji: An open-source platform for biological-image analysis. *Nat. Methods* **9**, 676–682.

Sebastian, D., Palacin, M., and Zorzano, A. (2017). Mitochondrial dynamics: Coupling mitochondrial fitness with healthy aging. *Trends Mol. Med.* **23**, 201–215.

Shen, Y., Ng, L. F., Low, N. P., Hagen, T., Gruber, J., and Inoue, T. (2016). *C. elegans* miro-1 mutation reduces the amount of mitochondria and extends life span. *PLoS One* **11**, e0153233.

Son, E. S., Kim, S. H., Ryter, S. W., Yeo, E. J., Kyung, S. Y., Kim, Y. J., Jeong, S. H., Lee, C. S., and Park, J. W. (2018). Quercetogetin

protects against cigarette smoke extract-induced apoptosis in epithelial cells by inhibiting mitophagy. *Toxicol. In Vitro* **48**, 170–178.

Subramaniam, S. R., and Chesselet, M. F. (2013). Mitochondrial dysfunction and oxidative stress in Parkinson's disease. *Prog. Neurobiol.* **106–107**, 17–32.

Sutphin, G. L., and Kaeberlein, M. (2009). Measuring *Caenorhabditis elegans* life span on solid media. *J. Vis. Exp.* **27**, e1152.

Tang, W. X., Wu, W. H., Qiu, H. Y., Bo, H., and Huang, S. M. (2013). Amelioration of rhabdomyolysis-induced renal mitochondrial injury and apoptosis through suppression of Drp-1 translocation. *J. Nephrol.* **26**, 1073–1082.

Tsang, W. Y., and Lemire, B. D. (2003). The role of mitochondria in the life of the nematode, *Caenorhabditis elegans*. *Biochim. Biophys. Acta* **1638**, 91–105.

Vásquez-Trincado, C., García-Carvajal, I., Pennanen, C., Parra, V., Hill, J. A., Rothermel, B. A., and Lavandero, S. (2016). Mitochondrial dynamics, mitophagy and cardiovascular disease. *J. Physiol.* **594**, 509–525.

Wang, G., Hazra, T. K., Mitra, S., Lee, H.-M., and Englander, E. W. (2000). Mitochondrial DNA damage and a hypoxic response are induced by $CoCl_2$ in rat neuronal PC12 cells. *Nucleic Acids Res.* **28**, 2135–2140.

Wang, P., Zhao, R., Yan, W., Zhang, X., Zhang, H., Xu, B., Chu, F., Han, Y., Li, G., Liu, W., *et al.* (2018). Neuroprotection by new ligustrazine-cinnamon acid derivatives on $CoCl_2$-induced apoptosis in differentiated PC12 cells. *Bioorg. Chem.* **77**, 360–369.

Wang, Y., Xie, W., and Wang, D. (2007). Transferable properties of multi-biological toxicity caused by cobalt exposure in *Caenorhabditis elegans*. *Environ. Toxicol. Chem.* **26**, 2405–2412.

Wu, Z., Zhang, M., Zhang, Z., Dong, W., Wang, Q., and Ren, J. (2018). Ratio of β-amyloid protein (aβ) and tau predicts the postoperative cognitive dysfunction on patients undergoing total hip/knee replacement surgery. *Exp. Ther. Med.* **15**, 878–884.

Yang, B., Cheng, H., Wang, L., Fu, J., Zhang, G., Guan, D., Qi, R., Gao, X., and Zhao, R. (2018). Protective roles of NRF2 signaling pathway in cobalt chloride-induced hypoxic cytotoxicity in human HaCaT keratinocytes. *Toxicol. Appl. Pharmacol.* **355**, 189–197.

Yang, C. C., Chen, D., Lee, S. S., and Walter, L. (2011). The dynamin-related protein DRP-1 and the insulin signaling pathway cooperate to modulate *Caenorhabditis elegans* longevity. *Aging Cell* **10**, 724–728.

Yoo, S. M., and Jung, Y. K. (2018). A molecular approach to mitophagy and mitochondrial dynamics. *Mol. Cells* **41**, 18–26.

Yoon, D. S., Lee, M. H., and Cha, D. S. (2018). Measurement of intracellular ROS in *Caenorhabditis elegans* using 2′,7′-dichlorodihydrofluorescein diacetate. *Bio Protoc.* **8**, e2774.

Yu, J., Yang, H., Fang, B., Zhang, Z., Wang, Y., and Dai, Y. (2018a). Mfat-1 transgene protects cultured adult neural stem cells against cobalt chloride-mediated hypoxic injury by activating Nrf2/ARE pathways. *J. Neurosci. Res.* **96**, 87–102.

Yu, Y., Li, W., Ren, L., Yang, C., Li, D., Han, X., Sun, Y., Lv, C., and Han, F. (2018b). Inhibition of autophagy enhanced cobalt chloride-induced apoptosis in rat alveolar type II epithelial cells. *Mol. Med. Rep.* **18**, 2124–2132.

Yuan, Z., Zhang, J., Huang, Y., Zhang, Y., Liu, W., Wang, G., Zhang, Q., Wang, G., Yang, Y., Li, H., *et al.* (2017). Nrf2 overexpression in mesenchymal stem cells induces stem-cell marker expression and enhances osteoblastic differentiation. *Biochem. Biophys. Res. Commun.* **491**, 228–235.

Zhang, Y., Chen, D., Smith, M. A., Zhang, B., and Pan, X. (2012). Selection of reliable reference genes in *Caenorhabditis elegans* for analysis of nanotoxicity. *PLoS One* **7**, e31849.

Zheng, F., Luo, Z., Zheng, C., Li, J., Zeng, J., Yang, H., Chen, J., Jin, Y., Aschner, M., Wu, S., *et al.* (2019). Comparison of the neurotoxicity associated with cobalt nanoparticles and cobalt chloride in Wistar rats. *Toxicol. Appl. Pharmacol.* **369**, 90–99.